

When does an active bath behave as an equilibrium one?

Shubhendu Shekhar Khali,^{1,*} Fernando Peruani,^{2,†} and Debasish Chaudhuri^{1,3,‡}

¹*Institute of Physics, Sachivalaya Marg, Bhubaneswar 751005, India*

²*LPTM, CY Cergy Paris Université, 2 avenue A. Chauvin, 95302 Cergy-Pontoise cedex, France*

³*Max-Planck Institute for the Physics of Complex Systems, Nöthnitzer Str. 38, 01187 Dresden, Germany*

(Dated: May 9, 2023)

Active baths are characterized by a non-Gaussian velocity distribution and a quadratic dependence with active velocity v_0 of the kinetic temperature and diffusion coefficient. While these results hold in over-damped active systems, inertial effects lead to normal velocity distributions, with kinetic temperature and diffusion coefficient increasing as $\sim v_0^\alpha$ with $1 < \alpha < 2$. Remarkably, the late-time diffusivity and mobility decrease with mass. Moreover, we show that the equilibrium Einstein relation is asymptotically recovered with inertia. In summary, the inertial mass restores an equilibrium-like behavior.

A fluid in equilibrium can be characterized as a heat bath in terms of its temperature, viscous drag, and diffusivity, obeying the Einstein relation [1]. Active Brownian particles (ABP), under certain conditions, can constitute a similar homogeneous and isotropic (as opposed to polar) active fluid – i.e., an active scalar fluid – in the presence of local energy dissipation and self-propulsion [2–7]. A question that naturally arises is to what extent such a fluid can be characterized as an *active* heat bath. The active nature of ABPs is determined by the self-propulsion speed v_0 and the orientational diffusivity of the heading direction D_r . This leads to a persistent random motion for individual ABPs, in dimension d , characterized by a late-time active diffusivity that scales as $\frac{v_0^2}{D_r d(d-1)}$. Early experiments on tracer particle dynamics in a bacterial suspension showed enhanced active diffusion [8, 9]. A higher density reduces diffusivity in equilibrium [10] but increases it in a non-equilibrium bacterial bath [8]. Various theoretical techniques were used to obtain the impact of an active bath on tracer particles [11–17]. Recent works have characterized ABP systems in terms of kinetic temperature, effective diffusivity, and viscous drag as a function of changing activity [18–25]. While diffusivity and kinetic temperature increase with activity, a non-monotonic variation of viscous drag has been predicted [22]. At the motility-induced phase separation (MIPS) [26–28], it was shown that the kinetic temperature could vary across a steady-state system with low (high) temperature characterizing the dense (dilute) phase [20]. However, it remains unclear to what extent such a description can be developed into a coherent self-consistent picture of active fluid, given, e.g., the breaking of time-reversal symmetry and the absence of equilibrium fluctuation-dissipation.

Despite tremendous progress in the study of active matter [2–6], until recently, relatively little attention was paid to the impact of inertia on the active matter except for [20, 29–34]. One reason for this is the extremely short time (~ 100 ns) and length scales (Angstrom) for the ballistic-diffusive crossover in colloidal particles.

However, for larger active elements, including birds, fish, and animals on the one hand, and artificial macro-sized robots [35–37] on the other hand, inertial effects can be substantial. This paper considers a homogeneous and isotropic fluid of active Brownian particles (ABP) and probes its active bath-like characteristics. A remarkable fact emerges: not only transient behaviors, even the asymptotic properties, including the effective diffusivity and mobility at the steady state, do depend on inertial mass, in sharp contrast to a non-interacting ABP gas. Furthermore, the strong non-Gaussian distribution of velocities returns towards equilibrium-like Gaussian for large mass. Finally, with increasing mass, the deviation from the equilibrium fluctuation-dissipation relation drops sharply. In summary, while activity amplifies non-equilibrium features, increasing the inertial mass brings the fluid back to equilibrium.

The model. – We consider N active Brownian particles (ABP) of mass m , a moment of inertia I , and diameter σ moving in a two-dimensional (2d) rectangular box of area $L_x \times L_y$ with periodic boundary conditions (thus, density $\rho = N/L_x L_y$). The particles self-propel in directions $\hat{n}_i = (\cos \theta_i, \sin \theta_i)$ with force $\mathbf{F}_{A,i} = \gamma_t v_0 \hat{n}_i$. Without interactions, this leads to a propulsion speed v_0 . The heading direction (i.e., θ_i) undergoes a long-time diffusion leading to an effective persistent motion. The inertial active dynamics evolve as

$$\begin{aligned} m\dot{\mathbf{v}}_i &= -\gamma_t \mathbf{v}_i + \mathbf{F}_i + \mathbf{F}_{A,i} + \gamma_t \sqrt{2D_t} \eta_i(t) \\ I\dot{\theta}_i &= -\gamma_r \dot{\theta}_i + \gamma_r \sqrt{2D_r} \zeta_i(t), \end{aligned} \quad (1)$$

where $\mathbf{F}_i = -\nabla_i \sum_j U(r_{ij})$, the symbols $\eta_i(t)$ and $\zeta_i(t)$ represent Gaussian white noises, and viscous drags, associated with translation and rotation, are described by $\gamma_t \mathbf{v}_i$ and $\gamma_r \dot{\theta}_i$, respectively. Interactions among particles are due to volume exclusion effects modeled via the Weeks-Chandler-Anderson potential: $U(r) = 4\epsilon[(\sigma/r)^{12} - (\sigma/r)^6] + \epsilon$ if the inter-particle separation $r < r_c = 2^{1/6} \sigma$ and $U(r) = 0$ otherwise. The units of length and energy are set by σ and ϵ , respectively. The rotational diffusivity D_r can have a non-thermal active

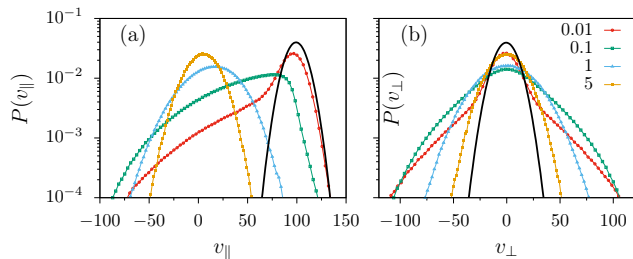


FIG. 1. *Velocity distributions in the particle frame.* Probability distributions of velocity components (a) parallel $P(v_{\parallel})$ and (b) perpendicular $P(v_{\perp})$ to the heading direction at $Pe = 100$ and for different M values indicated in the legend. Similarly, in $P(v_{\perp})$, non-Gaussian long tails disappear at high inertia. For comparison, we present the distribution functions for non-interacting particles at $M = 0.01$ using the solid black lines in both plots.

origin. Inertial relaxations in translation and rotation take time scales $\tau_I = m/\gamma_t$ and $\tau_d = I/\gamma_r$. Beyond τ_d , diffusion in the heading direction leads to a persistent motion with a bare persistence time $\tau_p = 1/D_r$, which sets the unit of time. Unless specified otherwise, we use an equilibrium heat bath with $D_t = 1.0\sigma^2 D_r$, and a small and constant $\tau_d = 0.33\tau_p$ [20]. We particularly focus on the impact of changing activity in terms of the Péclet number $Pe = v_0/(D_r\sigma)$ and that of the reduced mass using $M = \tau_I/\tau_p$. This system can undergo motility-induced phase separation (MIPS) for low enough M , and high enough Pe at a moderate density [20]. In order to fully characterize the properties of a homogeneous active bath, we fix the density to a low value, $\rho = 0.1$, corresponding to a packing fraction 8%, such that the system does not phase-separate even in the over-damped limit [7].

Results.— An increase in Pe , as expected, drives the system away from equilibrium. In Fig.1, we show the change in velocity distribution to reveal the impact of inertia. For this purpose, we consider the two components of the velocity, in the heading direction $v_{\parallel} = \mathbf{v} \cdot \hat{n}$ and perpendicular to it $v_{\perp} = (\mathbb{1} - \hat{n}\hat{n}) \cdot \mathbf{v}$. In 2d, v_{\perp} is a scalar. At small M , inertial lag is small. Despite that, $P(v_{\parallel})$ at $M = 0.01$ shows a long tail; see the red curve in Fig.1(a). This tail, which is absent in a system of non-interacting active particles, emerges due to enhanced frontal collision in the heading direction and the resultant inertial recoil. At larger inertia, secondary back collisions become prominent, symmetrizing the distribution to a Gaussian-like profile, e.g., at $M = 5$ [38]. The asymmetry in collisions will be scrutinized using a pair distribution function in Fig. 2. The $P(v_{\perp})$ distribution also shows inertial restoration of equilibrium-like behavior. The long non-Gaussian tails are observable at small M and disappear with an increase in M . The comparison with distributions obtained in the absence of interaction, black curves in Fig.1(a) and (b), shows that the non-

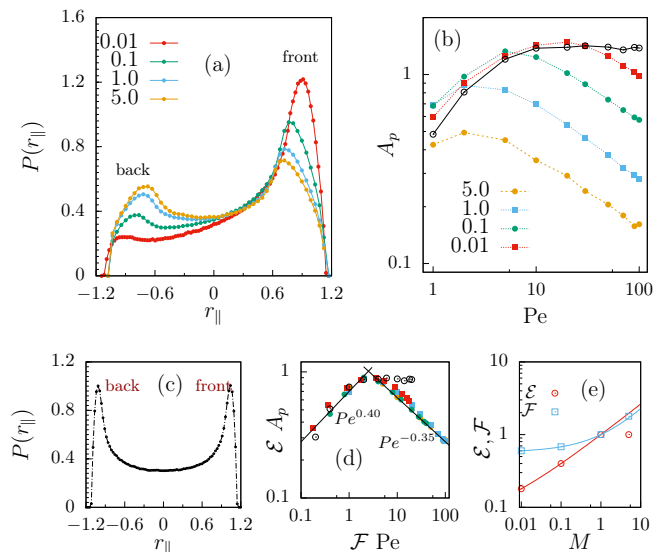


FIG. 2. *Pair distribution in the heading direction:* (a) $P(r_{\parallel})$ at $Pe = 100$ and various M values indicated in the legend. The fore-aft asymmetry decreases with increasing M . One gets a fully symmetric distribution at equilibrium, as shown in (c). (b) Variation of asymmetry parameter A_p as a function of Pe is shown for various M values indicated in the legend. (d) An approximate data collapse is obtained for inertial systems using appropriate rescaling of (b). (e) The variation of scale factors shown as a function of M . At large M , they show approximate dependencies $\mathcal{E} \sim M^{0.4}$ and $\mathcal{F} \sim M^{0.6}$.

Gaussian behaviors are strongly dependent on the inter-particle collisions. At high inertia, bouncing backward and forward from neighboring particles symmetrizes the distributions rendering them equilibrium-like shapes.

The impact of interaction manifests in the pair-distribution function in the heading direction, i.e., the probability $P(r_{\parallel})$ of finding a neighboring particle in direction \hat{n} ; see Fig.2. Due to enhanced frontal collision, more particles accumulate in front. Such accumulations in front and associated depletion wakes have been analyzed recently in overdamped dilute ABPs [39]. A peak in the back appears due to secondary back collisions experienced by inertial ABPs after frontal recoil. With increasing M , recoil increases, reducing the frontal accumulation and increasing the secondary collisions from the back – these affect the symmetrization of the pair distribution – restoring equilibrium-like behavior.

The asymmetry in the pair distribution is quantified in terms of the parameter A_p that measures the difference between the heights of the front and back peaks (Fig.2(b)). For fixed M , the asymmetry initially increases with Pe . For overdamped systems (black solid line denoting $M = 0$), the increase is followed by saturation in the absence of recoil. In contrast, in the presence of inertia, after the initial increase, A_p decreases with Pe . The data collapse in Fig.2(d) shows that at small

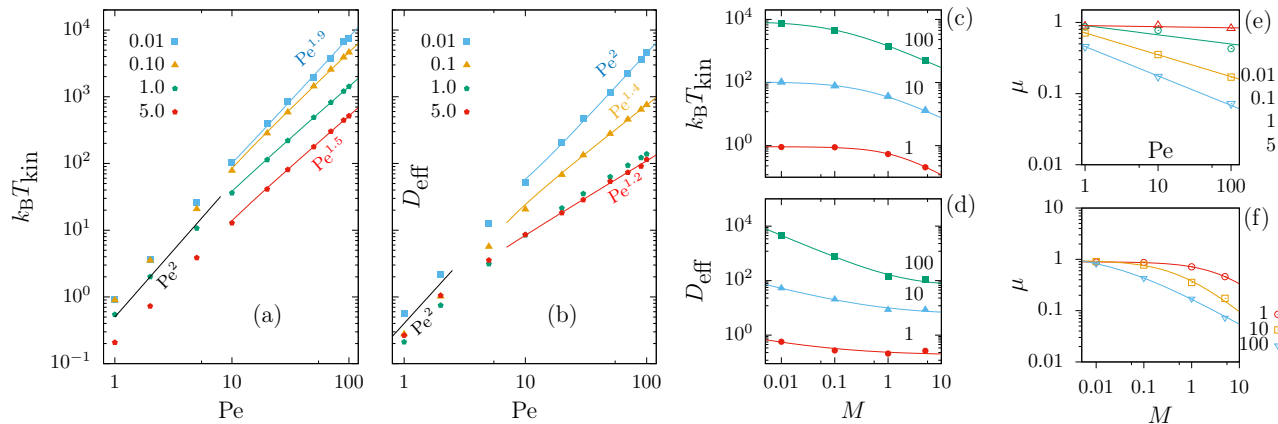


FIG. 3. (a) The increase in kinetic temperature $k_B T_{\text{kin}} = m\langle v^2 \rangle / 2$ with Pe is shown at various M values indicated in the legend. At large Pe, $k_B T_{\text{kin}} \sim Pe^{\alpha_k}$ with $\alpha_k = 1.90, 1.69, 1.54, 1.53$ at $M = 0.01, 0.1, 1, 5$. (b) The increase in effective diffusivity D_{eff} with Pe is shown at at various M values listed in the legend. Asymptotically it grows as $D_{\text{eff}} \sim Pe^{\alpha_d}$ with $\alpha_d = 1.98, 1.43, 1.13, 1.17$ at $M = 0.01, 0.1, 1, 5$. (c) At large M , the kinetic temperature decreases as $k_B T_{\text{kin}} \sim M^{-\gamma_k}$ with $\gamma_k = 1, 0.8, 0.75$ at $Pe = 1, 10$, and 100 . (d) D_{eff} reduces with M to saturate, and follows a scaling form $D_{\text{eff}} = \mathcal{B} + \mathcal{D} M^{-\gamma_d}$ with $\gamma_d = 0.43, 0.52, 0.81$ at $Pe = 1, 10$, and 100 . (e) The mobility μ as a function of Pe decreases as $\mu \sim Pe^{-\alpha_\mu}$ where $\alpha_\mu = 0.02, 0.13, 0.31, 0.41$ at $M = 0.01, 0.1, 1, 5$. (f) It decreases with M as $\mu \sim M^{-\gamma_\mu}$ at large M with $\gamma_\mu = 0.82, 0.77, 0.52$ at $Pe = 1, 10, 100$.

Pe, the asymmetry increases with Pe as $A_p \sim Pe^{0.4}$ and then decreases as $A_p \sim Pe^{-0.35}$. Such scaling properties are common to all inertial ABPs. The increase is due to enhanced frontal collisions associated with increased activity. The decrease is due to inertial recoil and is the reason behind the restoration of equilibrium-like behavior.

Another way of measuring how far the system is from equilibrium is given by the extent to which the equilibrium Einstein relation is violated $\mathcal{I} = |D_{\text{eff}} - \mu k_B T_{\text{kin}}|$, where μ is the particle mobility and T_{kin} the so-called kinetic energy [40, 41]. Following a tracer particle dynamics is a useful tool to characterize the properties of a bath [11, 12, 14–17]. In the presence of translational fluctuations, the impact of the activity on diffusivity at low Pe gets overshadowed by D_t . While these effects can be subtracted out, for simplicity and intending to understand the impact of the activity, in the following, we set $D_t = 0$. From the late-time behavior of the mean-squared displacements (MSD), we obtain the effective diffusivity D_{eff} . The kinetic temperature $k_B T_{\text{kin}}$ is readily obtainable from the velocity fluctuations. Using a separate numerical calculation of the change in velocity $\langle v_x \rangle$ of a test particle under an external force f_x , we obtain the mobility $\mu = (\partial \langle v_x \rangle / \partial f_x)_{f_x=0}$ around the non-equilibrium steady states of the ABPs. In the presence of an external force on the test particle, a local statistical reorganization of other ABPs follows. Such a reorganization depends on active speed and inertia, resulting in mobility variation. Using these, we obtain violation \mathcal{I} .

In Fig.3, we show the variations of kinetic temperature,

diffusivity, and mobility as a function of Pe and M . At large enough values of Pe and M , and they show the following scaling forms: (i) $k_B T_{\text{kin}} \sim Pe^{\alpha_k}$ and $k_B T_{\text{kin}} \sim M^{-\gamma_k}$, (ii) $D_{\text{eff}} \sim Pe^{\alpha_d}$ and $D_{\text{eff}} \sim M^{-\gamma_d}$, (iii) $\mu \sim Pe^{-\alpha_\mu}$ and $\mu \sim M^{-\gamma_\mu}$. Note that mobility decreases both with Pe and M , while the other quantities increase with Pe.

The kinetic temperature $k_B T_{\text{kin}} = m\langle v^2 \rangle / 2$ increases as a function of Pe (Fig.3(a)). The black solid line captures a Pe^2 scaling common to all M values at small Pe. The asymptotic behavior $k_B T_{\text{kin}} \sim Pe^{\alpha_k}$ at various M values shows how the exponent α_k decreases with M .

In Fig.3(b) we show how the effective diffusivity $D_{\text{eff}} \sim Pe^{\alpha_d}$ increases with Pe. At small Pe, $D_{\text{eff}} \sim Pe^2$ for all M . This behavior continues to all Pe in the limit of small inertia, $M = 0.01$, as in over-damped systems. However, with increasing inertia, the value of the growth exponent α_d decreases, and finally, $D_{\text{eff}} \sim Pe^{\alpha_d}$ becomes approximately linear with Pe at $M \gtrsim 1$.

In Fig.3(c) and (d), we show the M -dependency of the kinetic temperature and effective diffusivity. The kinetic temperature fits to the functional form $k_B T_{\text{kin}} = \mathcal{A}/(\mathcal{C} + M^{\gamma_k})$, such that at large M , they show a scaling form $k_B T_{\text{kin}} \sim M^{-\gamma_k}$ with the decay exponent γ_k decreasing with Pe. The effective diffusivity D_{eff} decays with M until it saturates, and follows a scaling form $D_{\text{eff}} = \mathcal{B} + \mathcal{D} M^{-\gamma_d}$ with the decay exponent γ_d increasing with Pe.

Finally, we consider the mobility μ . In the over-damped limit, μ is approximately independent of activity Pe ($M = 0.01$ in Fig.3(f)). This behavior agrees with the observation in Ref. [23] at low densities. However, in the

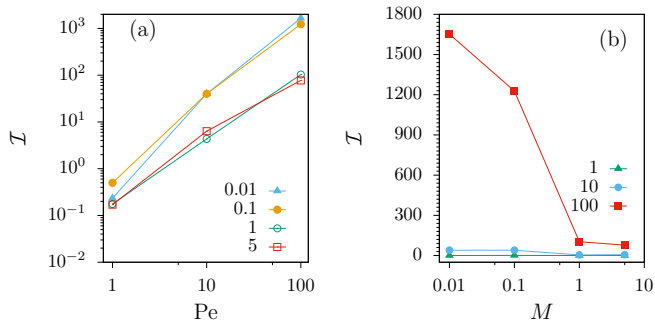


FIG. 4. The violation of equilibrium fluctuation-dissipation $\mathcal{I} = |D_{\text{eff}} - \mu k_B T_{\text{kin}}|$, a measure of how far the system is from equilibrium as a function of Pe and M , is shown in (a) and (b), respectively. \mathcal{I} increase with Pe as Pe^{α_d} or $Pe^{(\alpha_k - \alpha_\mu)}$. With M , it decreases to saturate at \mathcal{B} .

presence of inertia, mobility decreases with both Pe and M . At the larger activity, an increase in frontal collision frequency in the direction of external force increases the effective drag, leading to an effective thickening of the active fluid. Such a thickening is in qualitative agreement with Ref. [25], unlike the non-monotonic variation predicted in Ref. [22], and opposite to the active thinning predicted in Ref. [42]. As a function of the Pe , the mobility decreases as $\mu \sim Pe^{-\alpha_\mu}$ where the exponent α_μ itself increases with M (Fig.3(f)). The collision and recoil in inertial ABPs further increase the drag coefficient for higher inertial mass. The reduction of μ with M follows a form similar to that of the dependence of $k_B T_{\text{kin}}$ on M (Fig.3(c)), such that at large M $\mu \sim M^{-\gamma_\mu}$. Note that γ_μ also decreases with Pe .

With the help of these results, we find that the violation \mathcal{I} increases with Pe , but decreases with M . In particular, our findings indicate that $\mathcal{I} \sim |Pe^{\alpha_d} - Pe^{-\alpha_\mu + \alpha_k}|$, i.e., it can grow as Pe^{α_d} or $Pe^{\alpha_k - \alpha_\mu}$ depending on whether $\alpha_d > (\alpha_k - \alpha_\mu)$ or not (Fig.4(a)). On the other hand, $\mathcal{I} \sim |\mathcal{B} + \mathcal{D}M^{-\gamma_d} - M^{-(\gamma_\mu + \gamma_k)}|$ decreases with M to saturate at a Pe -dependent value \mathcal{B} (Fig.4(b)). Such a decrease is more significant at higher Pe . For small Pe , the system remains close to equilibrium for all M values.

Concluding remarks.— We have shown how the non-equilibrium properties of an active fluid consisting of ABPs, at a density far away from the onset of MIPS behave as a function of activity and inertial mass. While the departure from equilibrium gets pronounced with increasing Pe , i.e., activity, we found that inertial mass restores equilibrium-like properties. In particular, we showed that the non-Gaussian velocity distributions, the fore-aft asymmetry in the (heading-direction) pair distribution, and the absence of an Einstein fluctuation-dissipation relation between diffusivity, mobility, and kinetic temperature observed in active over-damped systems, crossover to their equilibrium counterparts with inertial mass. In short, we found that the inertial recoil

can effectively thermalize the active fluid. Remarkably, the late-time diffusivity and mobility of the bath depend on inertial mass, in contrast to free ABPs. The effective diffusivity and temperature grow with active velocity and decrease with inertial mass. In contrast, effective mobility decreases with mass and activity. Together, these findings show a reduction in the violation of equilibrium fluctuation-dissipation with increasing inertia. In summary, inertia brings back equilibrium-like behavior in the active fluid.

Numerical calculations were supported by SAMKHYA, the high-performance computing facility at the Institute of Physics, Bhubaneswar. D.C. thanks Arghya Majee for critical reading of the manuscript, C.Y. Cergy Paris Université for a Visiting Professorship which enabled the initiation of current work, SERB, India, for financial support through Grant No. MTR/2019/000750, and International Centre for Theoretical Sciences (ICTS-TIFR), Bangalore, for an Associateship. F.P. acknowledges financial support from C.Y. Initiative of Excellence (grant 'Investissements d'Avenir' ANR-16-IDEX-0008), INEX 2021 Ambition Project CollInt and Labex MME-DII, projects 2021-258 and 2021-297.

* shubhendu@iopb.res.in

† fernando.peruani@cyu.fr

‡ communicating author: debc@iopb.res.in

- [1] P. M. Chaikin and T. C. Lubensky, *Principles of Condensed Matter Physics* (Cambridge University Press, Cambridge, 2012).
- [2] C. Bechinger, R. Di Leonardo, H. Löwen, C. Reichhardt, G. Volpe, and G. Volpe, *Active Particles in Complex and Crowded Environments*, *Rev. Mod. Phys.* **88**, 045006 (2016), 1602.00081.
- [3] M. C. Marchetti, J. F. Joanny, S. Ramaswamy, T. B. Liverpool, J. Prost, M. Rao, and R. A. Simha, *Hydrodynamics of soft active matter*, *Rev. Mod. Phys.* **85**, 1143 (2013).
- [4] P. Romanczuk, M. Bär, W. Ebeling, B. Lindner, and L. Schimansky-Geier, *Active Brownian particles*, *Eur. Phys. J. Spec. Top.* **202**, 1 (2012).
- [5] S. Ramaswamy, *Active fluids*, *Nat. Rev. Phys.* **1**, 640 (2019).
- [6] G. Gompper, R. G. Winkler, T. Speck, A. Solon, C. Nardini, F. Peruani, H. Löwen, R. Golestanian, U. B. Kaupp, L. Alvarez, T. Kiorboe, E. Lauga, W. C. K. Poon, A. DeSimone, S. Muiños-Landin, A. Fischer, N. A. Söker, F. Cichos, R. Kapral, P. Gaspard, M. Ripoll, F. Sagues, A. Doostmohammadi, J. M. Yeomans, I. S. Aranson, C. Bechinger, H. Stark, C. K. Hemelrijk, F. J. Nedelec, T. Sarkar, T. Aryaksama, M. Lacroix, G. Duclos, V. Yashunsky, P. Silberzan, M. Arroyo, and S. Kale, *The 2020 motile active matter roadmap*, *J. Phys. Condens. Matter* **32**, 193001 (2020).
- [7] D. Richard, H. Löwen, and T. Speck, *Nucleation pathway and kinetics of phase-separating active Brownian particles*, *Soft Matter* **12**, 5257 (2016), 1602.07580.

- [8] X. L. Wu and A. Libchaber, Particle diffusion in a quasi-two-dimensional bacterial bath, *Phys. Rev. Lett.* **84**, 3017 (2000).
- [9] G. Grégoire, H. Chaté, and Y. Tu, Comment on “particle diffusion in a quasi-two-dimensional bacterial bath”, *Phys. Rev. Lett.* **86**, 556 (2001).
- [10] J. Lahtinen, T. Hjelt, T. Ala-Nissila, and Z. Chvoj, Diffusion of hard disks and rodlike molecules on surfaces, *Phys. Rev. E* **64**, 021204 (2001).
- [11] S. Ye, P. Liu, F. Ye, K. Chen, and M. Yang, Active noise experienced by a passive particle trapped in an active bath, *Soft Matter* **16**, 4655 (2020).
- [12] C. Maes, Fluctuating Motion in an Active Environment, *Phys. Rev. Lett.* **125**, 208001 (2020), 2005.13462.
- [13] C. Maes, Response Theory: A Trajectory-Based Approach, *Front. Phys.* **8**, 229 (2020), 2005.10503.
- [14] O. Granek, Y. Kafri, and J. Tailleur, The Anomalous Transport of Tracers in Active Baths, *Phys. Rev. Lett.* **129**, 38001 (2021), 2108.11970.
- [15] P. Rizkallah, A. Sarracino, O. Bénichou, and P. Illien, Microscopic Theory for the Diffusion of an Active Particle in a Crowded Environment, *Phys. Rev. Lett.* **128**, 038001 (2022), 2112.07312.
- [16] V. Démery, O. Bénichou, and H. Jacquin, Generalized Langevin equations for a driven tracer in dense soft colloids: Construction and applications, *New J. Phys.* **16**, 10.1088/1367-2630/16/5/053032 (2014).
- [17] V. Démery and D. S. Dean, Perturbative path-integral study of active- and passive-tracer diffusion in fluctuating fields, *Phys. Rev. E - Stat. Nonlinear, Soft Matter Phys.* **84**, 011148 (2011).
- [18] D. Loi, S. Mossa, and L. F. Cugliandolo, Effective temperature of active complex matter, *Soft Matter* **7**, 3726 (2011), 1012.2745.
- [19] L. F. Cugliandolo, G. Gonnella, and I. Petrelli, Effective Temperature in Active Brownian Particles, *Fluct. Noise Lett.* **18**, 1940008 (2019).
- [20] S. Mandal, B. Liebchen, and H. Löwen, Motility-Induced Temperature Difference in Coexisting Phases, *Phys. Rev. Lett.* **123**, 228001 (2019), 1902.06116.
- [21] J. Reichert and T. Voigtmann, Tracer dynamics in crowded active-particle suspensions, *Soft Matter* **17**, 10492 (2021), 2010.13769.
- [22] E. W. Burkholder and J. F. Brady, Nonlinear microrheology of active Brownian suspensions, *Soft Matter* **16**, 1034 (2020).
- [23] I. Petrelli, L. F. Cugliandolo, G. Gonnella, and A. Suma, Effective temperatures in inhomogeneous passive and active bidimensional Brownian particle systems, *Phys. Rev. E* **102**, 012609 (2020), 2005.02303.
- [24] L. Caprini and U. Marini Bettolo Marconi, Active matter at high density: Velocity distribution and kinetic temperature, *J. Chem. Phys.* **153**, 184901 (2020), 2009.07234.
- [25] C. Reichhardt and C. J. Reichhardt, Active microrheology in active matter systems: Mobility, intermittency, and avalanches, *Phys. Rev. E - Stat. Nonlinear, Soft Matter Phys.* **91**, 032313 (2015), 1409.1586.
- [26] Y. Fily and M. Marchetti, Athermal Phase Separation of Self-Propelled Particles with No Alignment, *Phys. Rev. Lett.* **108**, 235702 (2012).
- [27] G. S. Redner, M. F. Hagan, and A. Baskaran, Structure and Dynamics of a Phase-Separating Active Colloidal Fluid, *Phys. Rev. Lett.* **110**, 055701 (2013).
- [28] C. B. Caporusso, P. Digregorio, D. Levis, L. F. Cugliandolo, and G. Gonnella, Motility-Induced Microphase and Macrophase Separation in a Two-Dimensional Active Brownian Particle System, *Phys. Rev. Lett.* **125**, 178004 (2020).
- [29] C. Scholz, S. Jahanshahi, A. Ldov, and H. Löwen, Inertial delay of self-propelled particles, *Nat. Commun.* **9**, 5156 (2018), 1807.04357.
- [30] H. Löwen, Inertial effects of self-propelled particles: From active Brownian to active Langevin motion, *J. Chem. Phys.* **152**, 040901 (2020), 1910.13953.
- [31] J. Su, H. Jiang, and Z. Hou, Inertia-induced nucleation-like motility-induced phase separation, *New J. Phys.* **23**, 013005 (2021).
- [32] L. Caprini and U. Marini Bettolo Marconi, Inertial self-propelled particles, *J. Chem. Phys.* **154**, 024902 (2021), 2009.14032.
- [33] L. Hecht, S. Mandal, H. Löwen, and B. Liebchen, Active Refrigerators Powered by Inertia, *Phys. Rev. Lett.* **129**, 178001 (2022).
- [34] A. Solon and J. M. Horowitz, On the Einstein relation between mobility and diffusion coefficient in an active bath, *J. Phys. A Math. Theor.* **55**, 10.1088/1751-8121/ac5d82 (2022), 2203.05459.
- [35] O. Dauchot and V. Démery, Dynamics of a Self-Propelled Particle in a Harmonic Trap, *Phys. Rev. Lett.* **122**, 068002 (2019).
- [36] C. Scholz, M. Engel, and T. Pöschel, Rotating robots move collectively and self-organize, *Nat. Commun.* **9**, 931 (2018).
- [37] A. Deblais, T. Barois, T. Guerin, P.-H. Delville, R. Vaudaine, J. S. Lintuvuori, J.-F. Boudet, J.-C. Baret, and H. Kellay, Boundaries control collective dynamics of inertial self-propelled robots, *Physical review letters* **120**, 188002 (2018).
- [38] In the Supplementary Information provided online, we discuss further how M equilibrates the system, analyze the pair distribution function, show the calculation of mobility, diffusivity, and the behavior of scaling exponents describing kinetic temperature, effective diffusivity, and mobility.
- [39] A. Poncet, O. Bénichou, V. Démery, and D. Nishiguchi, Pair correlation of dilute active Brownian particles: From low-activity dipolar correction to high-activity algebraic depletion wings, *Phys. Rev. E* **103**, 012605 (2021), arXiv:2006.08202.
- [40] V. Blickle, T. Speck, C. Lutz, U. Seifert, and C. Bechinger, Einstein Relation Generalized to Nonequilibrium, *Phys. Rev. Lett.* **98**, 210601 (2007).
- [41] D. Chaudhuri and A. Chaudhuri, Modified fluctuation-dissipation and Einstein relation at nonequilibrium steady states, *Phys. Rev. E* **85**, 021102 (2012), 1201.4525.
- [42] A. Jayaram and T. Speck, Effective dynamics and fluctuations of a trapped probe moving in a fluid of active hard discs, (2023), arXiv:2302.08422.
- [43] L. Caprini, R. K. Gupta, and H. Löwen, Role of rotational inertia for collective phenomena in active matter, *Phys. Chem. Chem. Phys.* **24**, 24910 (2022).

Supplemental Information: When does an active bath behave as an equilibrium one?

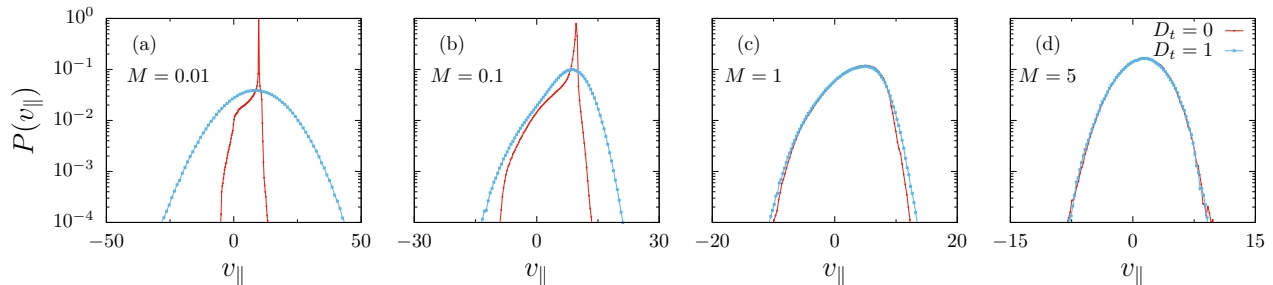


FIG. 5. Inertia brings back equilibrium-like features. The speed distributions in heading direction at $Pe = 10$ for different masses $M = 0.01$ in (a), $M = 0.1$ in (b), $M = 1$ in (c) and $M = 5$ in (d). In each plot, blue and red curves represent the results for $D_t = 1.0$ and 0.0 , respectively.

Inertial thermalization

As has been pointed out in the main text, with increasing M , the velocity distribution gets thermalized due to collisions and recoil. Here we supplement that finding with an independent measure in which we compare the velocity distribution in the heading direction in the presence ($D_t = 1$) and absence ($D_t = 0$) of a thermal bath (Fig.5). For small M , the two distributions are significantly different from each other. With increasing M , the distribution in the absence of thermal bath starts to *thermalize*, aided by relatively faster orientational relaxation of the heading direction during a slow inertial relaxation, and collisions from the front and secondary collisions from back after the frontal recoil. As a result, they start to come close to each other to merge at $M \gtrsim 1$.

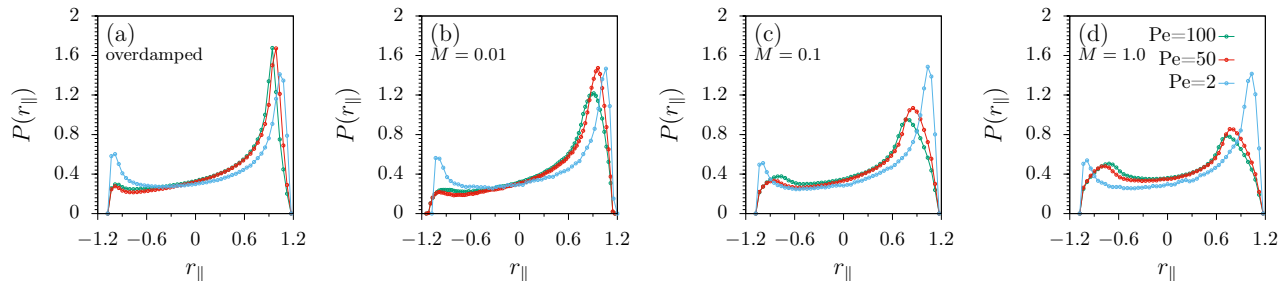


FIG. 6. Probability distribution of particle separation of interacting neighbors projected along the heading direction $P(r_{\parallel})$ at the system density $\rho = 0.1$ for $Pe = 2, 50$ and 100 . The results in (a) correspond to an over-damped system and in (b), (c), and (d) for an under-damped system with M values $= 0.01, 0.1$, and 1.0 , respectively. The common legend representing different Pe values is placed inside plot (d).

Pair distribution

In Fig.6, we show the distribution of particles around a test particle in its heading direction at $Pe=1, 10$, and 100 and inertia $M = 0, 0.01, 0.1, 1$. These distributions are used to calculate the asymmetry parameter A_p presented in the main text.

Mobility

To measure mobility, we apply an additional force F_x on the tagged particle and calculate its mean velocity along the same direction $\langle v_x \rangle$ for various F_x values. The mean velocity $\langle \delta v_x \rangle = \langle v_x \rangle|_{F_x} - \langle v_x \rangle|_{F_x=0}$ as a function of F_x is

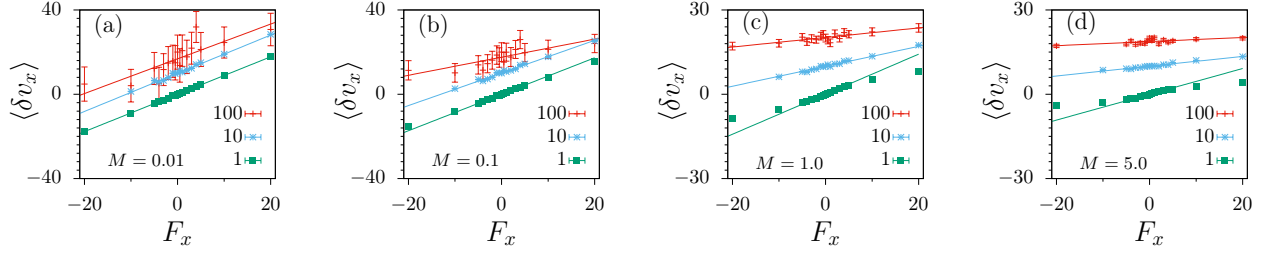


FIG. 7. The mean velocity of a tagged particle in response to the external force F_x is shown for $Pe = 1, 10,$ and 100 in (a) at $M = 0.01$, in (b) at $M = 0.1$, in (c) at $M = 1.0$ and in (d) at $M = 5$. The slope of the corresponding linear fits at $F_x = 0$ gives mobility $\mu = \lim_{F_x \rightarrow 0} \langle \delta v_x \rangle / F_x$. By definition $\langle \delta v_x \rangle = 0$ at $F_x = 0$. For the sake of clear visualization, each curve for $Pe = 10$ and 100 is shifted upwards.

shown in the figure 7. The slope of the linear fit for $\langle \delta v_x \rangle$ vs F_x curve near $F_x = 0$ gives mobility. In the overdamped regime $M = 0.01$, mobility does not show dependency on Pe as its value is observed to be the same $\mu \sim 0.9$ for $Pe = 1, 10,$ and 100 Fig.7 (a). In the underdamped limit ($M \geq 0.1$), mobility decreases with Pe , see Fig.7 (b),(c), (d).

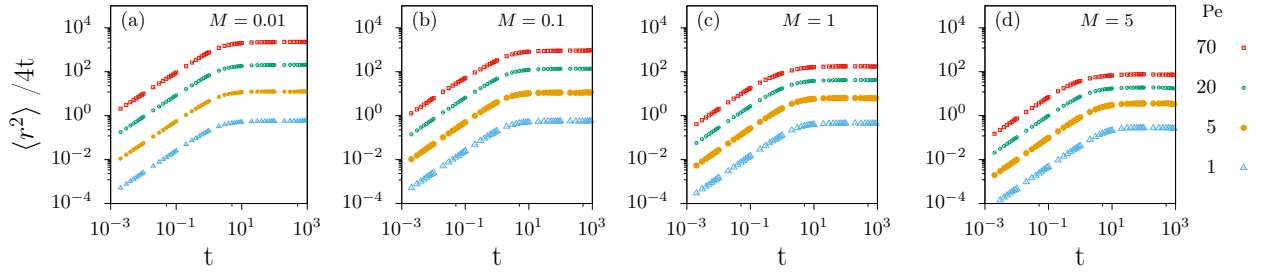


FIG. 8. Mean square displacement for $Pe = 1, 5, 20,$ and 70 in (a) at $M = 0.01$, in (b) at $M = 0.1$, in (c) at $M = 1.0$ and in (d) at $M = 5$. The common legend representing different Pe values is placed at the extreme right. These calculations are done for $D_t = 0$.

Mean-squared displacement

In Fig.8, we plot mean-squared displacement $\langle r^2 \rangle$ scaled by time t for different M and Pe values. All of them show ballistic to diffusive crossover at a time scale determined by the orientational persistence of the heading direction, a quantity that is kept constant in this paper. The asymptotic diffusivities $D_{\text{eff}} = \lim_{t \rightarrow \infty} \langle r^2 \rangle / 4t$ are obtained from these graphs and used in the main text.

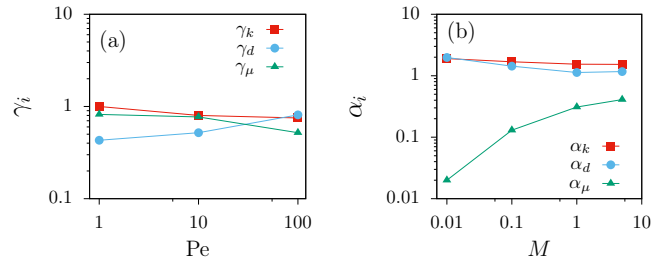


FIG. 9. Scaling exponents γ_i and α_i used in Fig.4 are presented as a function of Pe (a) and M (b), respectively. $i = k, d, \mu$ represent exponents of kinetic energy, diffusion, and mobility.

Scaling exponents

The variations of scaling exponents determining the Pe and M dependence of kinematic temperature, effective diffusivity, and mobility are shown in Fig.9.